Applied Physics Letters ACCEPTED MANUSCRIPT

This is the author's peer reviewed, accepted manuscript. However, the online version of record will be different from this version once it has been copyedited and typeset.

PLEASE CITE THIS ARTICLE AS DOI: 10.1063/5.0105412

AIP Publishing

Physical mechanisms for delaying condensation freezing on grooved and sintered wicking surfaces

Emily M. Stallbaumer-Cyr, Melanie M. Derby, Amy R. Betz*

Alan C. Levin Department of Mechanical and Nuclear Engineering, Carl R. Ice College of Engineering, Kansas State University, Manhattan, KS 66506, USA

*Corresponding author: arbetz@ksu.edu

ABSTRACT

Heat pipes are passive heat transfer devices crucial for systems on spacecraft; however, they can freeze when exposed to extreme cold temperatures. The research on freezing mechanisms on wicked surfaces, such as those found in heat pipes, is limited. Surface characteristics, including surface topography, have been found to impact freezing. This work investigates freezing mechanisms on wicks during condensation freezing. Experiments were conducted in an environmental chamber at 22°C and 60% relative humidity on three types of surfaces (i.e., plain copper, sintered heat pipe wicks, and grooved heat pipe wicks). The plain copper surface tended to freeze via ice bridging – consistent with other literature – before the grooved and sintered wicks at an average freezing time of 4.6 minutes with average droplet diameters of 141.9 ± 58.1 µm at freezing. The grooved surface also froze via ice bridging but required, on average, almost double the length of time the plain copper surface took to freeze, 8.3 minutes with average droplet diameters of 60.5 ± 27.9 µm at freezing. Bridges could not form between grooves so initial freezing for each groove was stochastic. The sintered wick's surface could not propagate solely by ice bridging due to its topography, but also employed stochastic freezing and cascade freezing, which prompted more varied freezing times and an average of 10.9 minutes with average droplet diameters of 97.4 ± 32.9 µm at freezing. The topography of the wicked surfaces influenced the location of droplet nucleation and, therefore, the ability for droplet-to-droplet interaction during the freezing process.

Heat pipes are a critical component in heat management systems, from laptops [1] to spacecraft [2]; the usefulness of heat pipes comes from their ability to passively transfer heat without additional equipment [1, 3-6]. For space applications, heat pipes can be exposed to the freezing temperatures of space – resulting in the solidification of the working fluid [6, 7], thereby reducing or preventing function [6, 8], decreasing performance [9], or damaging the wick [7, 9]. Current heat pipe freezing research focuses primarily on start-up from a frozen state [4, 6, 7, 10, 11] and liquid control methods to prevent ice plugs (i.e. gas-charged heat pipes) [4, 6, 8, 11].

Applied Physics Letters ACCEPTED MANUSCRIPT

This is the author's peer reviewed, accepted manuscript. However, the online version of record will be different from this version once it has been copyedited and typeset.

PLEASE CITE THIS ARTICLE AS DOI: 10.1063/5.0105412

AIP Publishing

Limited data exist on the freezing process in the heat pipes. Current research on freezing via condensation (i.e., condensation frosting) focuses primarily on flat surfaces [12-14] or surfaces designed to delay freezing or promote easy ice removal, such as coatings and hydrophobic surfaces [15-19], micropillars, microgrooves [20-23], chemical etching, and nanopillars [21, 23-26]. Surface characteristics, such as hydrophobicity [15, 23], surface topography [22, 23, 26-28], surface roughness [21, 29], and surface tension [21, 29] affect behaviors such as droplet nucleation, droplet sizes, time freezing begins, and freezing propagation.

The research objectives of this work are to investigate and compare condensation freezing on commercial heat pipe wicks (i.e., grooved and sintered wicks) and a plain copper surface. This research will illuminate freezing mechanisms, quantify freezing times, and explain freezing propagation on complex three-dimensional surfaces. This fundamental understanding of freezing mechanisms in three dimensions is vital to the future design of heat pipes where performance is not prevented or impeded by freezing.

The Gibbs free energy barrier must be overcome for initial condensation nucleation and freezing to begin on the surface; the Gibbs free energy barrier is impacted by the surface tension and the droplet diameter (i.e., larger droplets take more energy to freeze)[12, 16, 25, 30-32]. The change in Gibbs free energy equation is [12, 30]:

$$\Delta G = V_I \Delta \tilde{g}_V + \sigma_{IL} A_{IL} + (\sigma_{Iw} - \sigma_{wL}) A_{Iw}$$

where V_I is the volume of the ice embryo, $\tilde{g}_V$ is the change in energy per volume between water and ice, A is the contact area, and σ is the surface tension; the subscripts V, I, L, and w stand for volumetric, ice, liquid water, and the wall of the surface, respectively. Changes in the droplet volume, contact angle, and contact area of the droplet will change the Gibbs free energy barrier, thereby changing when freezing occurs. Increasing the volume of the ice embryo will also increase the contact area between the ice and liquid phases and/or the contact area between the ice and the wall of the surface, resulting in an overall increase of the change in Gibbs free energy. Altering the surface's wettability to increase the surface tension between the droplet and the surface will also result in an increase of the change in Gibbs free energy. Additionally, increasing the surface tension will likely result in an increased area between the droplet and the surface, further increasing the change in Gibbs free energy. Increasing the change in Gibbs free energy will require more energy for droplets to change from liquid to ice. However, surface modifications to change the Gibbs free energy are limited for heat pipes due to the necessity of the wick to transport liquids.

Applied Physics Letters ACCEPTED MANUSCRIPT
This is the author's peer reviewed, accepted manuscript. However, the online version of record will be different from this version once it has been copyedited and typeset.
PLEASE CITE THIS ARTICLE AS DOI: 10.1063/5.0105412
AIP Publishing

On surfaces, the initial freezing frequently occurs on either the edges or on defects/rougher locations on the surface, due to the lowered Gibbs free energy [21, 32, 33]. After the initial freezing, the freezing front propagates along the surfaces via frozen droplets' interactions with liquid droplets. Ice bridging is the main propagation mechanism for the majority of surfaces investigated; water from a liquid droplet evaporates due to the proximity of a frozen droplet and the difference in pressure between the liquid droplet and the frozen droplet [12, 32, 34-36]. The water vapor reaches the frozen droplet, causing vapor to condense and freeze, thereby creating a bridge between the two droplets. When the bridge reaches the neighboring liquid droplet, it freezes that droplet; however, if the bridging parameter, S^* is greater than one, the droplet will evaporate completely before the ice bridge reaches the liquid droplet, creating a dry zone [12, 34, 36, 37]. Dry zones are areas in which frozen droplets and the neighboring droplets cannot interact. The bridging parameter is defined as $S^* = L_{max}/d$ where L_{max} is the largest distance between the two droplets and d is the liquid droplet's diameter [34, 36, 37]. Frost halos occur when a droplet initially freezes; the vapor pressure of the ice is greater than the vapor pressure of the liquid, thereby expelling vapor from the freezing droplet and condensing on the surrounding surface where the new droplets freeze [12, 35, 36]. Similar to frost halos, cascade freezing occurs when vapor is expelled from the freezing droplet; however, the vapor, along with airborne dust, impinges on the neighboring droplets and induces freezing instead of impinging and condensing on the surface [35, 38].

For this research, a plain copper surface, two copper sintered wick surfaces (Adv Thermal Solutions, ATSHP-F8L150S45W-455, flat heat pipe, 9.45mm wide), and two copper grooved wick surfaces (Adv Thermal Solutions, ATS-HPD6L300G30W-00, round heat pipe, 6.0mm in diameter) were investigated. The sintered and grooved wick surfaces are from commercially available heat pipes; the heat pipes were cut in half lengthwise and split into 25-mm-long sections. The surfaces were placed on a Peltier cooler under a Confocal Microscope. The surface temperature was set to -5°C and the surfaces were observed for approximately 1-hour, sufficient time for the surfaces to completely freeze. The freezing start time is the first instance of observable solidification of condensed water droplets and the freezing end time corresponds to the time when the observed surface is completely covered in ice. The freezing times were determined by observing locations near the center of the surfaces. The length of freezing is taken as the freezing end time minus the freezing start time [39]. Further discussion on the Experimental Apparatus can be found in the supplemental material.

Freezing was observed on five surfaces [i.e., Plain, Grooved 1 (G1), Grooved 2 (G2), Sintered 1 (S1), and Sintered 2 (S2)]; five replicates were conducted for each surface. The freezing times are shown in Figure 1. Additional experiments were performed on the Grooved 2, Sintered 2, and Plain copper surfaces at

Applied Physics Letters ACCEPTED MANUSCRIPT
This is the author's peer reviewed, accepted manuscript. However, the online version of record will be different from this version once it has been copyedited and typeset.
PLEASE CITE THIS ARTICLE AS DOI: 10.1063/5.0105412
AIP Publishing

increased magnification to determine the size of droplets at freezing. Freezing is determined by the change in optical properties (transmittance and reflectance) of droplets. The histograms of droplet diameters at the time of freezing are shown in Figure 2. On the plain copper surface, freezing began after 6.3 minutes, on average. After freezing was initiated on the plain copper surface, the observed surface completely froze after an average of 4.6 minutes. The droplet diameters at freezing ranged widely on the plain copper surface, from 43.6 µm–418.5 µm, with an average diameter of 141.9 ± 58.1 µm (Figure 2A). Ice bridging is identified as the main freezing mechanism propelling the freezing front on the plain copper surface (Figure 3) (Multimedia view), consistent with previous literature regarding freezing fronts on smooth surfaces [15, 26, 34, 36]. Figure 3A depicts a frozen droplet on the plain surface that, as shown in Figure 3B, grows an ice bridge to its neighboring droplet, initiating freezing in the neighboring droplet, as depicted in Figure 2D. The newly frozen droplet then also creates an ice bridge to initiate freezing in one of its neighboring droplets (Figure 3C).

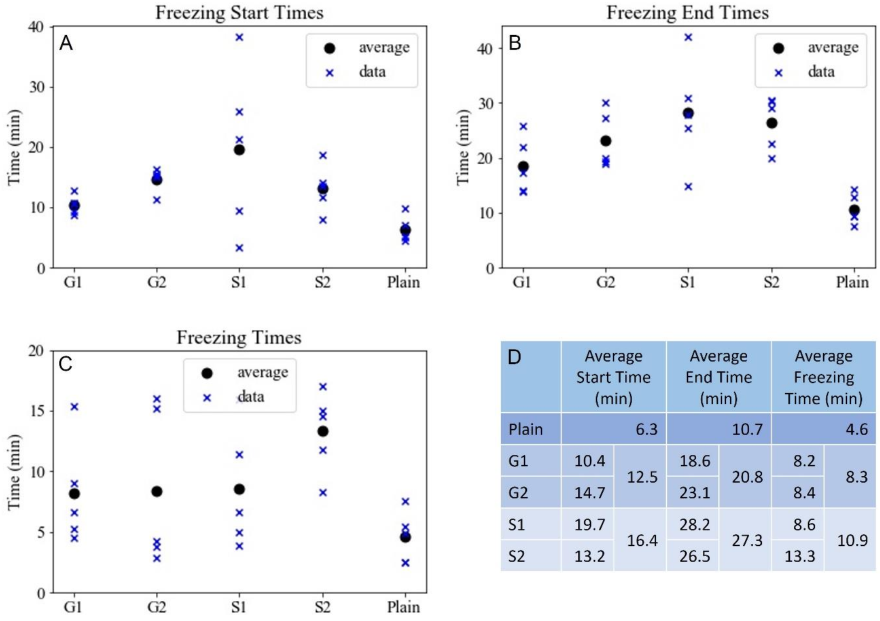

D	Average Start Time (min)		Average End Time (min)		Average Freezing Time (min)	
Plain	6.3		10.7		4.6	
G1	10.4	12.5	18.6	20.8	8.2	8.3
G2	14.7		23.1		8.4	
S1	19.7	16.4	28.2	27.3	8.6	10.9
S2	13.2		26.5		13.3	

Figure 1: Graphs and table indicating the start, end, and freezing times of the surfaces. (A) The freezing start times of the individual replicates on the different surfaces. (B) The freezing end times of the individual replicates on the different surfaces. (C) The time it takes the surfaces to freeze from start to finish. (D) A table of the averages of the start time, end time, and freezing time.

Applied Physics Letters ACCEPTED MANUSCRIPT

This is the author's peer reviewed, accepted manuscript. However, the online version of record will be different from this version once it has been copyedited and typeset.

PLEASE CITE THIS ARTICLE AS DOI: 10.1063/5.0105412

AIP Publishing

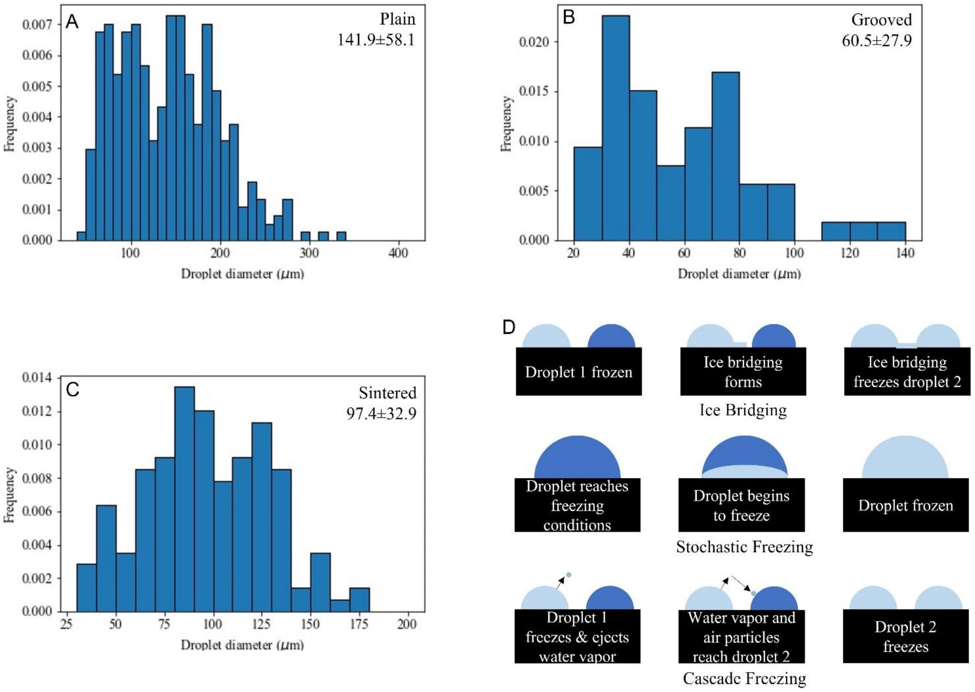

Figure 2: Histograms of the size of frozen droplets from 5 experiments on the (A) Plain copper surface with a frozen droplet diameter range from 43.6 μm–418.5 μm, (B) Grooved 2 with a frozen droplet diameter range from 24.9 μm–142.7 μm, and (C) Sintered 2 with a frozen droplet diameter range from 33.9–203.1 μm. (D) Schematic of three droplet freezing mechanisms, ice bridging, stochastic freezing, and cascade freezing.

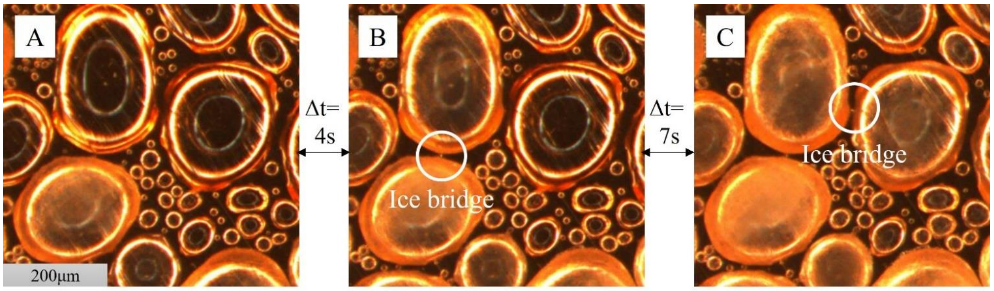

Figure 3: Droplets freezing on the plain surface (Multimedia view). (A) a droplet freezing before bridging to its neighbor. (B) the frozen droplet bridging to its neighbor causing it to freeze. (C) the newly frozen droplet bridging to its neighbor causing it to freeze.

AIP Publishing

Similar freezing mechanisms were observed on the grooved wicks. The grooved wicks began to freeze at 12.5 minutes on average, the most consistent start time of the three surfaces. Once the grooved wick surfaces initiated freezing, the whole observed surface (i.e. the top or portion furthest from the Peltier cooler of the grooves) was frozen, on average, after 8.3 minutes. The droplet diameters at freezing ranged from 24.9 µm–142.7 µm, with an average diameter of 60.5 ± 27.9 µm; the grooved wick had the most consistent droplet diameters (Figure 2B). The droplet width is constrained by the width of the grooves (i.e., approximately 86 µm); those droplets which exceed the width of the groove are fewer and grow oblong. The freezing front propagated along individual grooves using ice bridging, similarly to the plain copper surface, as shown in Figure 4 (Multimedia view). However, as shown in Figure 4C, ice may attempt to bridge the in-plane distance between two grooves, but it does not cover the distance before the groove begins to freeze (Figure 4D). After the second groove freezes, the ice bridge does not continue to grow as it no longer has a water source to draw from. The distance between grooves is greater than the width of the grooves, therefore larger than the majority of the frozen droplet diameters on the grooved wick; the bridging parameter S^* is greater than one. The formation of an ice bridge between droplets on neighboring grooves will not be successful; furthermore, the space between the grooves creates a dry zone that cannot be overcome [36]. This indicates that each groove must initiate freezing and the grooves function as their own independent surface. Since the droplets cannot communicate with droplets on neighboring grooves, the average freezing start time for the observable grooved wick is longer and more inconsistent than the plain copper surface.

Applied Physics Letters ACCEPTED MANUSCRIPT
This is the author's peer reviewed, accepted manuscript. However, the online version of record will be different from this version once it has been copyedited and typeset.
PLEASE CITE THIS ARTICLE AS DOI: 10.1063/5.0105412
AIP Publishing

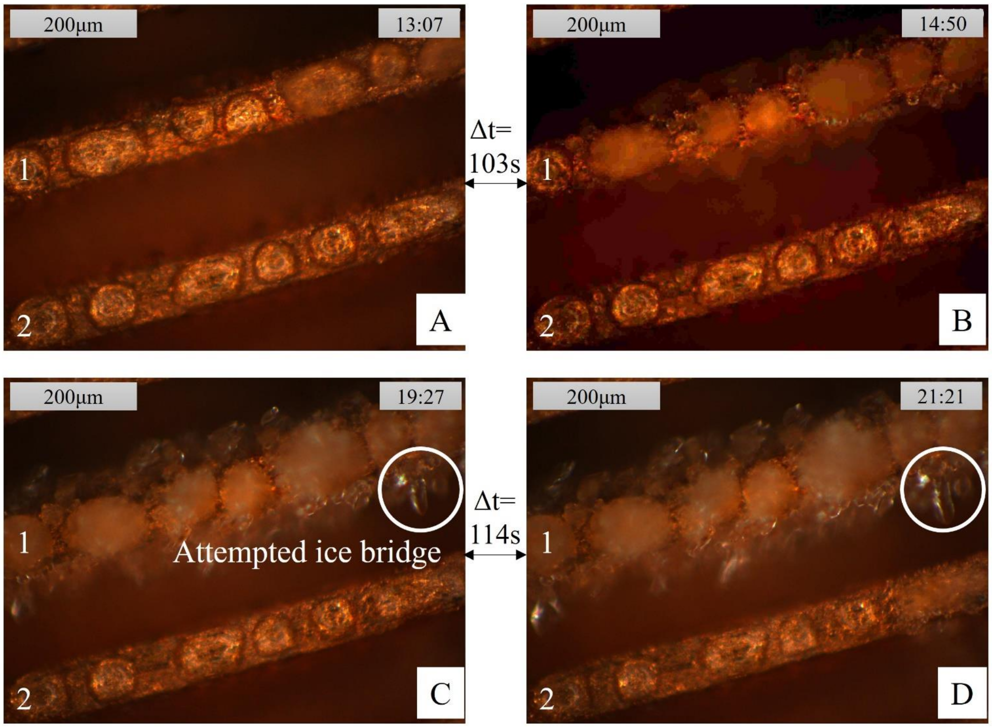

Figure 4: Droplets freezing on the top of two grooves in a grooved wick (i.e. the portion of the groove furthest from the Peltier cooler). (A) The droplets have begun to freeze on one of the grooves, (B) the droplets on groove 1 are completely frozen, (C) almost 4.5 minutes after the droplets on groove 1 froze, the droplets on groove 2 remain as water, though the ice is attempting to reach out in the creation of an in-plane ice bridge, (D) a little under 5.5 minutes after the droplets on groove 1 are completely frozen, groove 2 begins to freeze, even though the ice has not bridged the gap between the grooves, additionally, the ice attempting to bridge stops growing without a water source (Multimedia view).

The sintered wicks began to freeze at 16.4 minutes, on average. Once the sintered wick surfaces initiated freezing, the entire observed surface was frozen, on average, after 10.9 minutes. The droplet diameters at freezing ranged from 33.9–203.1 µm, with an average diameter of 97.4 ± 32.9 µm (Figure 2C). The particles of sintered wicks dictate the location of droplet nucleation and growth. As seen in Figure 1, the freezing times for the sintered wick varied from 3.9 to 17.0 minutes; more than and averaged longer than that of the plain copper surface and grooved wick. It was also observed that an increased start time did not result in an increased freezing time. Previous results showed that freezing start times correlate with total time to freezing [26]. This can be explained by the structure of the sintered wick. Due to the nature of sintering, the sintered wick has 'voids', i.e. space without particles. Images of the sintered wick were run

AIP Publishing

through Python image processing code and the percentage of voids to total area was calculated (supplemental material: Image Analysis of Voids in Sintered Wicks). The amount of void area in an observed area varied due to the randomness of the sintered particles along the wick. As the amount of void area increased, the time it took for the wick to freeze also tended to increase. Decreasing the amount of area for droplets to form limits the number of droplets that can interact with one another. Additionally, decreasing the total area for droplets to form also decreases the size droplets can grow, limiting the distance droplets can transverse to interact with one another. These limits impact the freezing front propagation, increasing the time it takes the surface to freeze. The freezing front must be able to bridge the voids, travel around the voids, or stochastic freezing must occur for the freezing front to continue. While the amount of void area impacts the freezing front, so does the length and width of the void or the occurrence of 'peninsulas' of sintered particles stretching into the void. These can allow for droplets to be close enough to communicate across voids. The freezing front on the sintered wicks is propagated by ice bridging, stochastic freezing of droplets, and cascade freezing.

Ice bridging can only occur on the sintered wick where sintered particles exist such that $S^* < 1$ for the droplets, as shown in Figure 5A-C (Multimedia view). Figure 5A depicts a liquid water droplet whose neighboring droplets have frozen. Figure 5B depicts the ice bridges growing from the frozen droplets to the liquid droplet, and Figure 5C depicts the ice bridges reaching the liquid droplet and inducing freezing. Due to the location of the sintered particles creating the wick, the distance between the droplets was too large for the freezing front to propagate predominantly by ice bridging. Similar to the grooved wick surface, the sintered wick has multiple locations where $S^* > 1$; the location of the sintered particles creates voids or dry zones between the droplets where droplets cannot form and therefore ice bridging propagation cannot occur. Additionally, due to these dry zone voids, the freezing propagation tends to move from various frame edges towards the center, instead of propagating in one direction, similar to the micropillar surfaces with geometrical defects found in [27].

The sintered wick also froze via stochastic freezing – the water droplets reached freezing conditions (i.e., the Gibbs free energy barrier is overcome [30, 36]), shown in Figure 5D-F (Multimedia view) and depicted in Figure 2D. These droplets may overcome the Gibbs free energy barrier due to the roughness and edges of the sintered particles. Figure 5D depicts a liquid droplet with some frozen droplets on the sintered particles surrounding it, light is reflected on the droplet. Without any of the neighboring frozen droplets interacting with the liquid droplet, the liquid droplet freezes; the droplet loses reflectance (Figure 5E) and transmittance (Figure 5F) as it freezes.

Applied Physics Letters ACCEPTED MANUSCRIPT

This is the author's peer reviewed, accepted manuscript. However, the online version of record will be different from this version once it has been copyedited and typeset.

PLEASE CITE THIS ARTICLE AS DOI: 10.1063/5.0105412

AIP Publishing

The last method of freezing front propagation along the sintered wick surface is cascade freezing, depicted in Figure 2D. A freezing droplet initiates freezing in close neighboring droplets ~less than 1 second after beginning to freeze; the neighboring droplets begin to freeze following the initial droplet but before an ice bridge would be able to begin forming) (Figure 5G-H) (Multimedia view) [35, 38]. Figure 5G depicts a group of three liquid droplets not experiencing any interaction with the surrounding frozen droplets. The middle droplet in Figure 5 begins freezing and expels water vapor that impinges on the two neighboring liquid droplets, resulting in the liquid droplets freezing (Figure 5I).

Applied Physics Letters ACCEPTED MANUSCRIPT

This is the author's peer reviewed, accepted manuscript. However, the online version of record will be different from this version once it has been copyedited and typeset.

PLEASE CITE THIS ARTICLE AS DOI: 10.1063/5.0105412

AIP Publishing

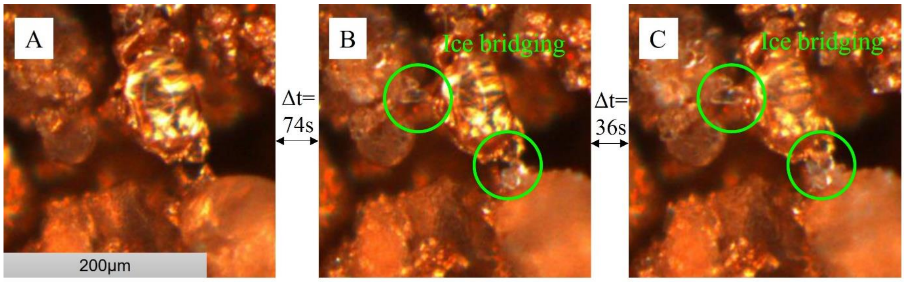
A
200μm
Δt= 74s
B
Ice bridging
Δt= 36s
C
Ice bridging

Ice Bridging

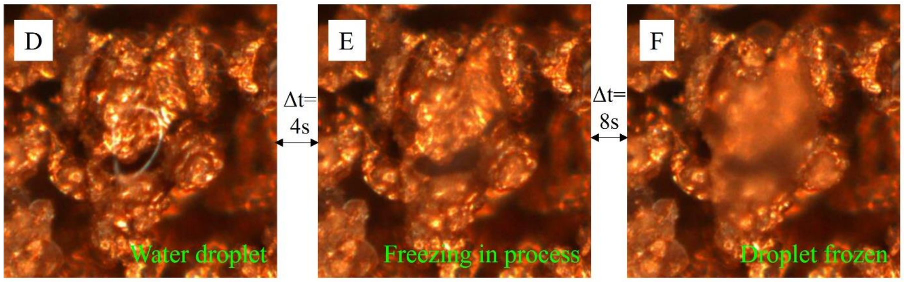
D
Water droplet
Δt= 4s
E
Freezing in process
Δt= 8s
F
Droplet frozen

Stochastic Freezing

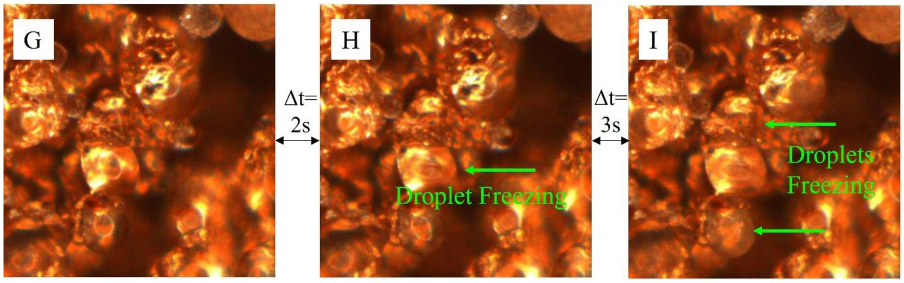
G
Δt= 2s
H
Droplet Freezing
Δt= 3s
I
Droplets Freezing

Cascade Freezing

Figure 5: The mechanisms of droplets freezing on the sintered wick. (A-C) show ice bridging (Multimedia view), (D-F) shows a droplet freezing despite experiencing no interactions from the droplets surrounding it via stochastic freezing; the freezing process is observed by the loss of reflectance between (D) and (E) and loss of transmittance between (E) and (F) (Multimedia view), (G-I) show droplets freezing due to cascade freezing; the two additional droplets freeze within a second of the first and are seen in supplementary video (multimedia view).

Stochastic freezing is not the predominant method of freezing a surface due to the time it takes for droplets to overcome the Gibbs free energy [12, 16, 25, 30-32]. On the observed surfaces, the average freezing start times were 6.3 minutes on the plain, 12.5 minutes on the grooved, and 16.4 minutes on the sintered. The droplets on the observed surface could not overcome the Gibbs free energy before freezing

Applied Physics Letters ACCEPTED MANUSCRIPT
This is the author's peer reviewed, accepted manuscript. However, the online version of record will be different from this version once it has been copyedited and typeset.
PLEASE CITE THIS ARTICLE AS DOI: 10.1063/5.0105412
AIP Publishing

propagation mechanisms reached the observed surface. The freezing began on the edges of the observed surfaces, indicating freezing from interaction with the droplets outside of the observed surface; a droplet in an area of lower Gibbs free energy (e.g. a surface edge) froze allowing propagation to the observed surface [12]. Ice bridging has been observed to propagate swiftly on surfaces, the speed of ice bridging propagation relies on the length of bridges required [16, 34]. Ice bridging on the plain copper surface with close droplets created ice bridges within 4 and 7 seconds in Figure 3 (Multimedia view). Haque et al. [16] correlated the bridge length to bridging time for droplets on graphene surfaces, the longer the bridge the longer it took to bridge the gap, with the lengths between 3 μm and 23 μm and corresponding times between a few seconds and 60 seconds. The average times for the observed surfaces to completely freeze were 4.6 minutes and 8.3 minutes, respectively. Both the plain and grooved surfaces froze primarily via ice bridging. While ice bridging takes a few seconds, cascade freezing occurs within milli- or deci-seconds [35, 38]. The plain surface droplets can interact with each other and freeze via droplet bridging; however, the droplets on one groove cannot interact with the droplets on a neighboring groove. Similarly, due to voids on the sintered surface, there are areas where the droplets cannot interact, slowing the freezing front (supplemental material: Image Analysis of Voids in Sintered Wicks). On the sintered wick, in the supplementary videos corresponding to Figure 5G-I, the neighboring droplets are seen experiencing cascade freezing following the freezing of the first droplet.

Understanding the freezing mechanisms on wicking surfaces can lead to wick designs that can mitigate the damaging effects of heat pipe freezing. The topography of the surfaces has greater impacts on the freezing time by influencing the freezing mechanisms and the speed at which the freezing front can propagate. The plain copper surface can employ ice bridging across its entire length, with minimal interference. Therefore, a majority of the droplets formed on the surface resulted in a bridging parameter of less than one. While the grooved surfaces employ ice bridging as well ($S^* < 1$), the droplet-to-droplet interaction is restricted to droplets along the same groove. Droplet bridging from the top of one groove to another fails due to the S^*>1, thereby increasing the time for the grooved surface to freeze, as each groove must freeze individually. The sintered surfaces employ a mixture of ice bridging ($S^* < 1$), stochastic freezing, and cascade freezing. The freezing times on the sintered wick were the most varied of the three surfaces, had the most varied freezing start times, as well as the longest freezing start and end times, as a result of the differing area taken up by voids. The varied freezing times result from the dry zone voids ($S^* > 1$) created by the sintered particles and the sintered particles themselves acting as surface defects or edges; additionally, the surface topography results in varied freezing methods of different length and time scales – ice bridging, stochastic freezing, and cascade freezing. This research shows the opportunity

Applied Physics Letters ACCEPTED MANUSCRIPT

This is the author's peer reviewed, accepted manuscript. However, the online version of record will be different from this version once it has been copyedited and typeset.

PLEASE CITE THIS ARTICLE AS DOI: 10.1063/5.0105412

AIP Publishing

for optimization of heat pipe geometry to take advantage of the different time and length scales associated with the different freezing mechanisms to prevent harmful effects of freezing. The void structure and surface energy could be tailored to simultaneously allow for wicking the liquid state but prevent ice bridging and cascade freezing mechanism.

Supplementary Material

Additional detail describing the experimental apparatus and explaining the image analysis are provided in the supplementary materials.

Author Declarations

This project was supported and funded by the NSF Research Traineeship Rural Resiliency 1828571. The authors gratefully acknowledge the Institute for Environmental Research at KSU for the use of their environmental chambers.

Conflict of Interests

The authors have no conflicts to disclose.

Data Availability

The data that support the findings of this study are openly available in Mendeley Data at

http://doi.org/10.17632/x4jtph9hzw.2 [40]

References

[1] R. Cai, P. Bai, H. Wang, Y. Luo, X. Chen, G. Wu*, et al.*, "Experimental investigation of the heat transfer performance of a novel double independent chambers casing heat pipe applied for heat dissipation at low temperatures," *Applied Thermal Engineering,* vol. 188, p. 116508, 2021.

[2] K. Shukla, "Heat pipe for aerospace applications—an overview," *Journal of Electronics Cooling and Thermal Control,* vol. 5, p. 1, 2015.

[3] G. Y. Eastman, "The heat pipe," *Scientific American,* vol. 218, pp. 38-47, 1968.

[4] A. Faghri, "Heat pipes: review, opportunities and challenges," *Frontiers in Heat Pipes (FHP),* vol. 5, 2014.

[5] W. Chen, "A Multi-Environment Thermal Control System With Freeze-Tolerant Radiator," in *43rd International Conference on Environmental Systems*, 2013, p. 3354.

[6] M. Ababneh, C. Tarau, W. Anderson, A. Alvarez-Hernandez, S. Ortega, J. Farmer*, et al.*, "Demonstration of Copper-Water Heat Pipes Embedded in High Conductivity (HiK™) Plates in the Advanced Passive Thermal eXperiment (APTx) on the International Space Station," 2018.

[7] K.-L. Lee, C. Tarau, and W. G. Anderson, "Titanium water heat pipe radiators for space fission system thermal management," in *Proceedings of the Joint 19th International Heat Pipe Conference and 13th International Heat Pipe Symposium*, 2018.

Applied Physics Letters ACCEPTED MANUSCRIPT
This is the author's peer reviewed, accepted manuscript. However, the online version of record will be different from this version once it has been copyedited and typeset.
PLEASE CITE THIS ARTICLE AS DOI: 10.1063/5.0105412
AIP Publishing

[8] J. Ku, L. Ottenstein, and A. Krimchansky, "Investigation of Freeze/Thaw Cycles of a Gas-Charged Heat Pipe," in *43rd AIAA Thermophysics Conference*, 2012, p. 2749.
[9] J. Cepeda-Rizo, "The Problem of Freezing of Copper Water Heat Pipes," presented at the Thirty-Fourth Annual Workshop on Mathematical Problems in Industry, 2018.
[10] A. Faghri, "Frozen start-up behavior of low-temperature heat pipes," *International journal of heat and mass transfer,* vol. 35, pp. 1681-1694, 1992.
[11] J. Ochterbeck and G. Peterson, "Freeze/thaw characteristics of a copper/water heat pipe-Effects ofnoncondensible gas charge," *Journal of thermophysics and heat transfer,* vol. 7, pp. 127-132, 1993.
[12] S. Nath and J. B. Boreyko, "On localized vapor pressure gradients governing condensation and frost phenomena," *Langmuir,* vol. 32, pp. 8350-8365, 2016.
[13] K.-S. Lee, S. Jhee, and D.-K. Yang, "Prediction of the frost formation on a cold flat surface," *International journal of heat and mass transfer,* vol. 46, pp. 3789-3796, 2003.
[14] C. J. Hermes, R. O. Piucco, J. R. Barbosa Jr, and C. Melo, "A study of frost growth and densification on flat surfaces," *Experimental Thermal and Fluid Science,* vol. 33, pp. 371-379, 2009.
[15] M. R. Haque and A. R. Betz, "Frost formation on aluminum and hydrophobic surfaces," in *International Conference on Nanochannels, Microchannels, and Minichannels*, 2018, p. V001T04A001.
[16] M. R. Haque, S. R. Das, and A. R. Betz, "Experimental investigation of condensation and freezing phenomena on hydrophilic and hydrophobic graphene coating," *Applied Thermal Engineering,* vol. 160, p. 113987, 2019.
[17] Y. Zhang, M. R. Klittich, M. Gao, and A. Dhinojwala, "Delaying frost formation by controlling surface chemistry of carbon nanotube-coated steel surfaces," *ACS applied materials & interfaces,* vol. 9, pp. 6512-6519, 2017.
[18] Z.-J. Wang, D.-J. Kwon, K. L. DeVries, and J.-M. Park, "Frost formation and anti-icing performance of a hydrophobic coating on aluminum," *Experimental Thermal and Fluid Science,* vol. 60, pp. 132-137, 2015.
[19] M. R. Haque, *Understanding and controlling condensation and frosting phenomena on engineered surfaces*: Kansas State University, 2019.
[20] M. A. Muntaha, M. M. Haider, and M. A. Rahman, "Modelling of frost formation and growth on microstuctured surface," in *AIP Conference Proceedings*, 2016, p. 050042.
[21] P. Hao, C. Lv, and X. Zhang, "Freezing of sessile water droplets on surfaces with various roughness and wettability," *Applied physics letters,* vol. 104, p. 161609, 2014.
[22] Y. Shen, H. Zou, and S. Wang, "Condensation frosting on micropillar surfaces–effect of microscale roughness on ice propagation," *Langmuir,* vol. 36, pp. 13563-13574, 2020.
[23] W. Sheng, Y. Pei, X. Li, P. Ming, and W. Zhao, "Effect of surface characteristics on condensate droplets growth," *Applied Thermal Engineering,* vol. 173, p. 115260, 2020.
[24] P. Eberle, M. K. Tiwari, T. Maitra, and D. Poulikakos, "Rational nanostructuring of surfaces for extraordinary icephobicity," *Nanoscale,* vol. 6, pp. 4874-4881, 2014.
[25] M. Rejaul Haque, C. Zhu, C. Qu, E. C. Kinzel, and A. Rachel Betz, "Experimental Investigation of Condensation and Freezing Phenomenon on Hydrophilic and Hydrophobic Titanium Nanopillared Glass Surfaces," *Heat Transfer Engineering,* vol. 42, pp. 533-548, 2021.
[26] R. Bohm, M. R. Haque, C. Qu, E. C. Kinzel, and A. R. Betz, "Accelerated freezing due to droplet pinning on a nanopillared surface," *AIP Advances,* vol. 8, p. 125228, 2018.
[27] Y. Zhao, R. Wang, and C. Yang, "Interdroplet freezing wave propagation of condensation frosting on micropillar patterned superhydrophobic surfaces of varying pitches," *International Journal of Heat and Mass Transfer,* vol. 108, pp. 1048-1056, 2017.

Applied Physics Letters ACCEPTED MANUSCRIPT

This is the author's peer reviewed, accepted manuscript. However, the online version of record will be different from this version once it has been copyedited and typeset.

PLEASE CITE THIS ARTICLE AS DOI: 10.1063/5.0105412

AIP Publishing

[28] Y. Zhao and C. Yang, "Frost spreading on microscale wettability/morphology patterned surfaces," *Applied Thermal Engineering,* vol. 121, pp. 136-145, 2017.

[29] F. M. Ruiz-Cabello, S. Bermúdez-Romero, P. F. Ibanez-Ibanez, M. Cabrerizo-Vilchez, and M. Rodríguez-Valverde, "Freezing delay of sessile drops: Probing the impact of contact angle, surface roughness and thermal conductivity," *Applied Surface Science,* vol. 537, p. 147964, 2021.

[30] B. Na and R. L. Webb, "A fundamental understanding of factors affecting frost nucleation," *International Journal of Heat and Mass Transfer,* vol. 46, pp. 3797-3808, 2003.

[31] A. S. Van Dyke, D. Collard, M. M. Derby, and A. R. Betz, "Droplet coalescence and freezing on hydrophilic, hydrophobic, and biphilic surfaces," *Applied Physics Letters,* vol. 107, p. 141602, 2015.

[32] M.-H. Kim, H. Kim, K.-S. Lee, and D. R. Kim, "Frosting characteristics on hydrophobic and superhydrophobic surfaces: A review," *Energy Conversion and Management,* vol. 138, pp. 1-11, 2017.

[33] J. McCormick and J. Westwater, "Nucleation sites for dropwise condensation," *Chemical Engineering Science,* vol. 20, pp. 1021-1036, 1965.

[34] S. Nath, S. F. Ahmadi, and J. B. Boreyko, "How ice bridges the gap," *Soft Matter,* vol. 16, pp. 1156-1161, 2020.

[35] A. A. Yancheshme, G. Momen, and R. J. Aminabadi, "Mechanisms of ice formation and propagation on superhydrophobic surfaces: A review," *Advances in Colloid and Interface Science,* vol. 279, p. 102155, 2020.

[36] S. Nath, S. F. Ahmadi, and J. B. Boreyko, "A review of condensation frosting," *Nanoscale and Microscale Thermophysical Engineering,* vol. 21, pp. 81-101, 2017.

[37] J. B. Boreyko, R. R. Hansen, K. R. Murphy, S. Nath, S. T. Retterer, and C. P. Collier, "Controlling condensation and frost growth with chemical micropatterns," *Scientific reports,* vol. 6, pp. 1-15, 2016.

[38] G. Graeber, V. Dolder, T. M. Schutzius, and D. Poulikakos, "Cascade freezing of supercooled water droplet collectives," *ACS nano,* vol. 12, pp. 11274-11281, 2018.

[39] E. Stallbaumer, A. Cernas, A. Betz, and M. Derby, "Ice Formation due to Condensation of Moist Air on Commercial Wicks," in *International Conference on Nanochannels, Microchannels, and Minichannels*, 2020, p. V001T03A004.

[40] E. Stallbaumer-Cyr, M. Derby, and A. Betz, "Condensation freezing times for commercially available heat pipe wicks," V2 ed. Mendeley Data, 2022.

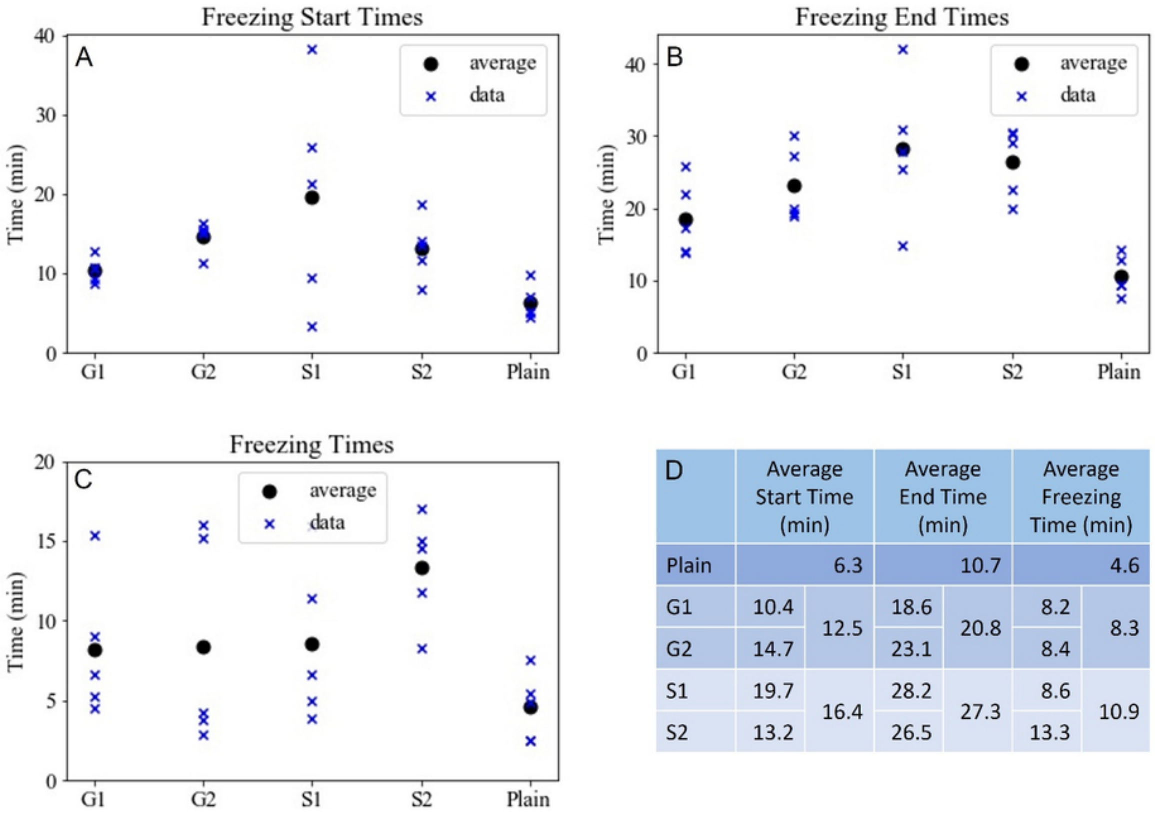

D	Average Start Time (min)		Average End Time (min)		Average Freezing Time (min)	
Plain		6.3		10.7		4.6
G1	10.4	12.5	18.6	20.8	8.2	8.3
G2	14.7		23.1		8.4	
S1	19.7	16.4	28.2	27.3	8.6	10.9
S2	13.2		26.5		13.3	

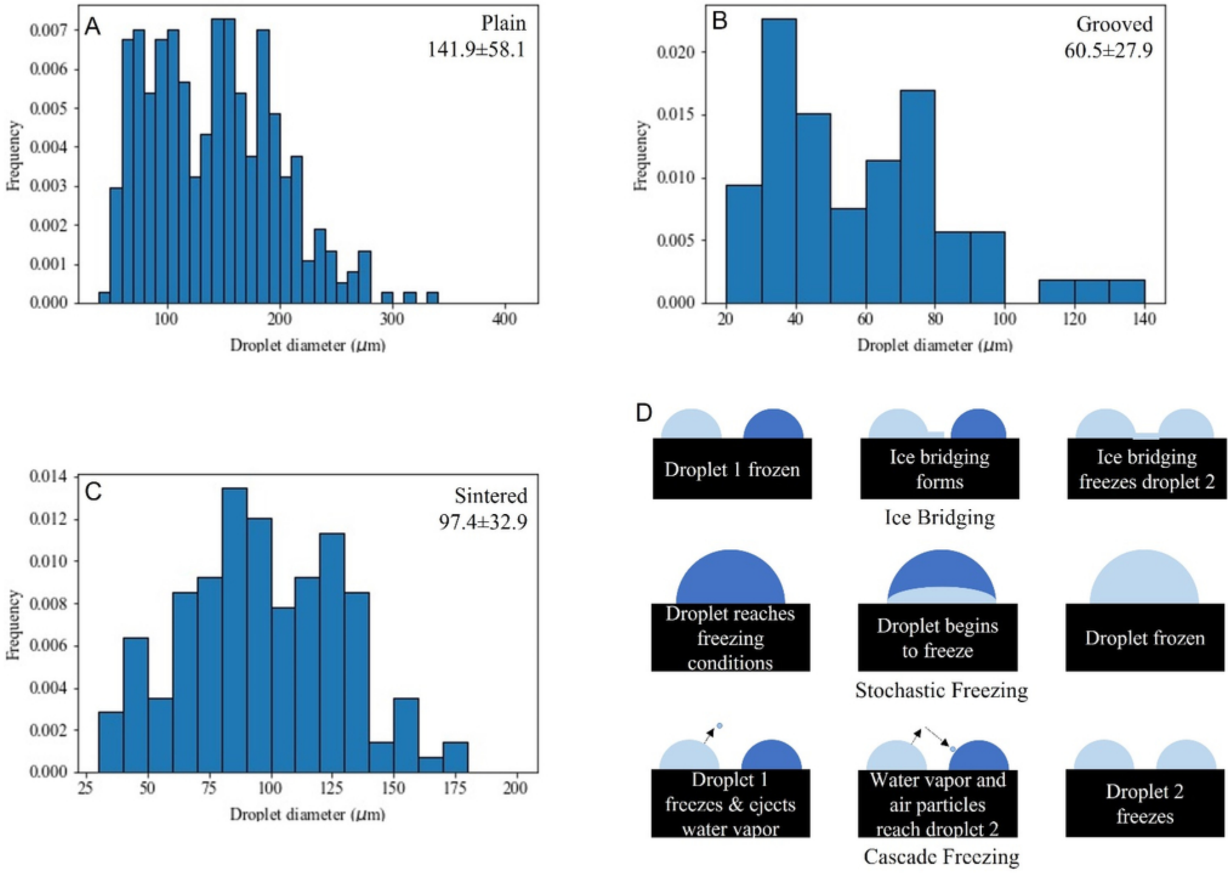
A
Plain
141.9±58.1
Frequency
0.000
0.001
0.002
0.003
0.004
0.005
0.006
0.007
100
200
300
400
Droplet diameter (μm)
B
Grooved
60.5±27.9
Frequency
0.000
0.005
0.010
0.015
0.020
20
40
60
80
100
120
140
Droplet diameter (μm)
C
Sintered
97.4±32.9
Frequency
0.000
0.002
0.004
0.006
0.008
0.010
0.012
0.014
25
50
75
100
125
150
175
200
Droplet diameter (μm)
D
Droplet 1 frozen
Ice bridging forms
Ice bridging freezes droplet 2
Ice Bridging
Droplet reaches freezing conditions
Droplet begins to freeze
Droplet frozen
Stochastic Freezing
Droplet 1 freezes & ejects water vapor
Water vapor and air particles reach droplet 2
Droplet 2 freezes
Cascade Freezing

PLEASE CITE THIS ARTICLE AS DOI: 10.1063/5.0105412

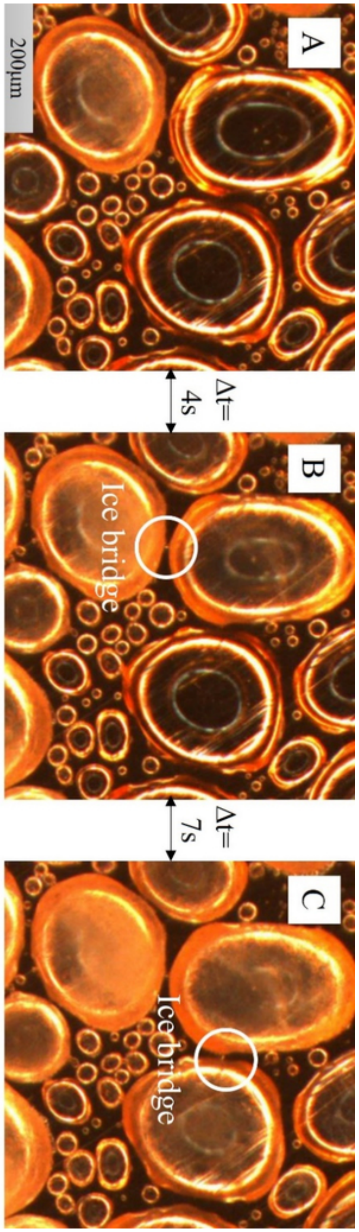
A
200μm
Δt=
4s
B
Ice bridge
Δt=
7s
C
Ice bridge

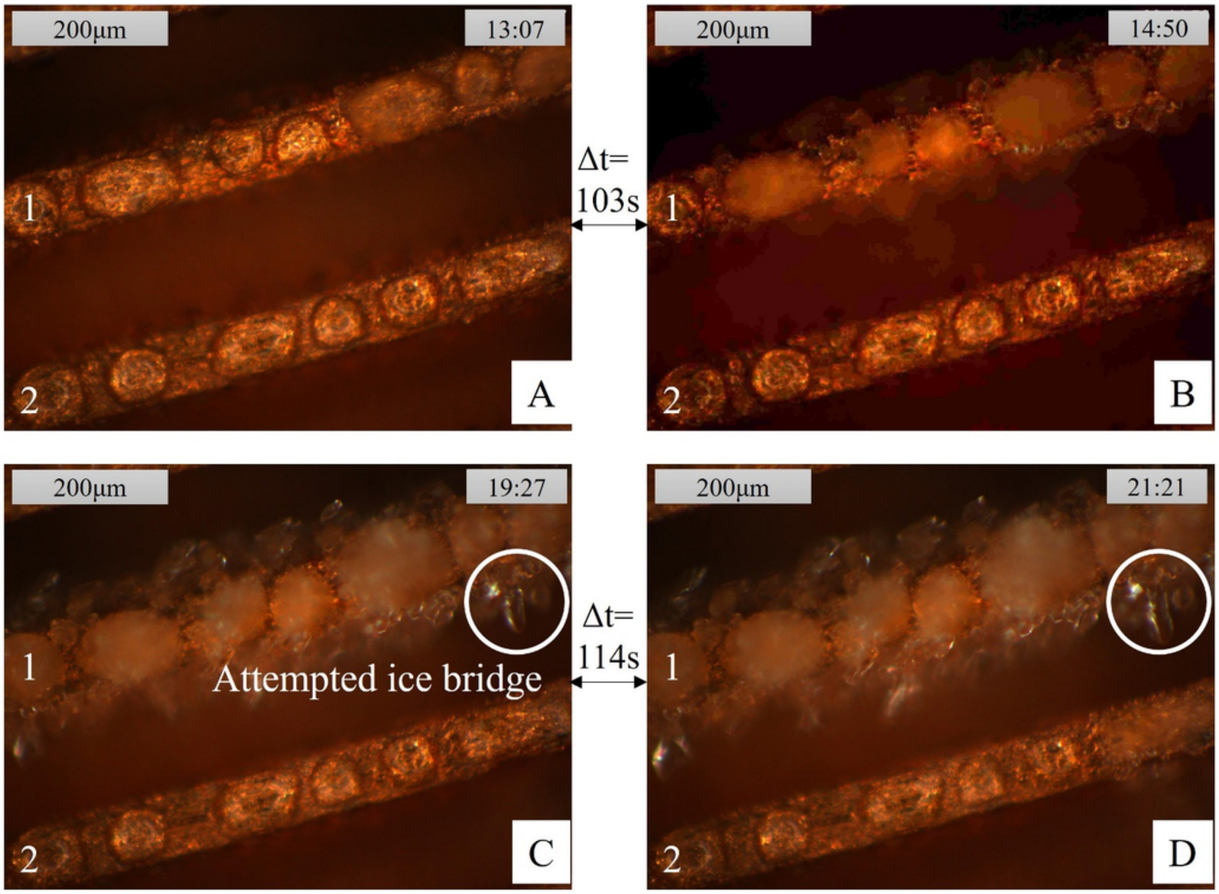
200µm
13:07
1
2
A
Δt=
103s
200µm
14:50
1
2
B
200µm
19:27
1
Attempted ice bridge
2
C
Δt=
114s
200µm
21:21
1
2
D

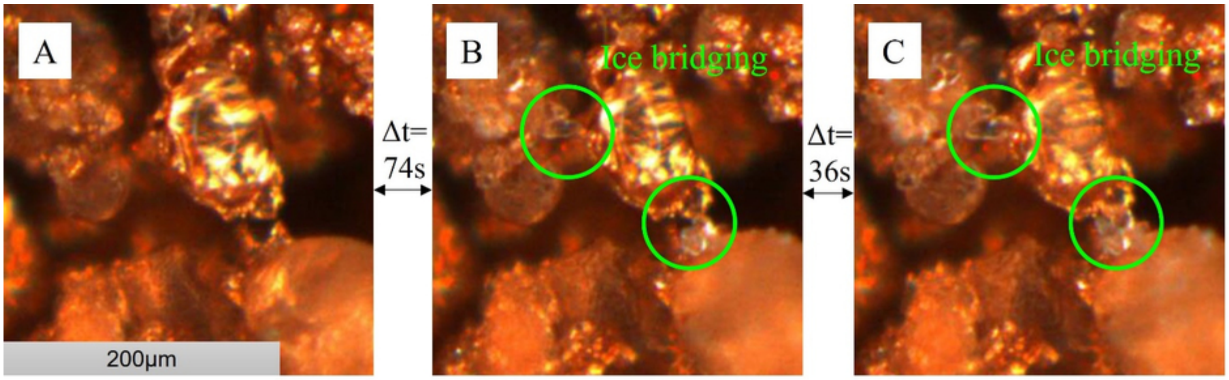
A
200μm
Δt=
74s
B
Ice bridging
Δt=
36s
C
Ice bridging

Ice Bridging

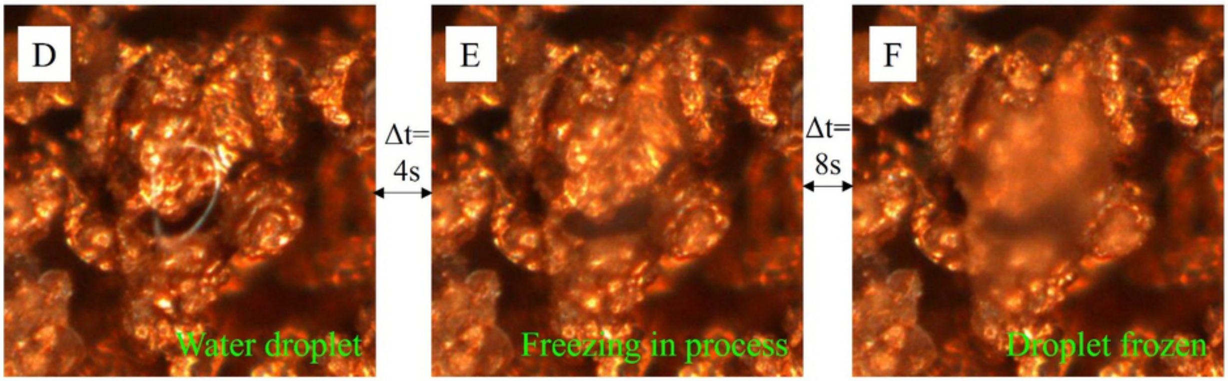
D
Water droplet
Δt=
4s
E
Freezing in process
Δt=
8s
F
Droplet frozen

Stochastic Freezing

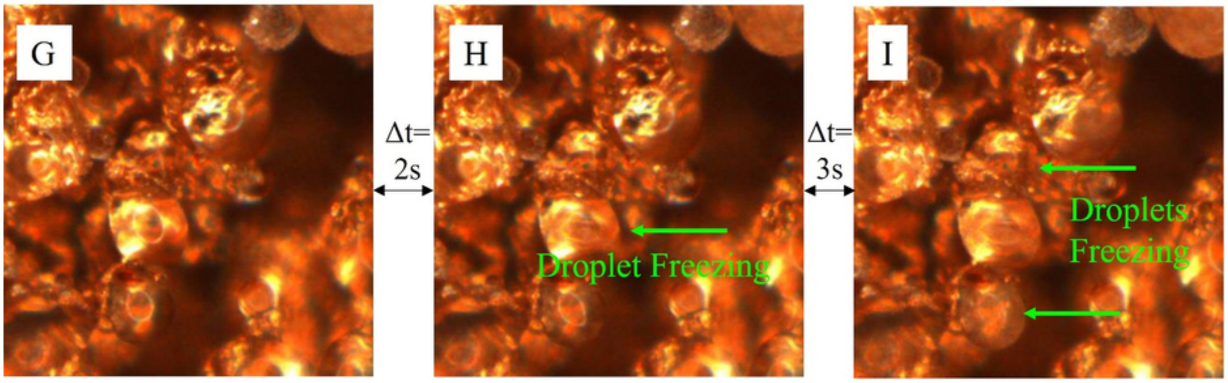
G
Δt=
2s
H
Droplet Freezing
Δt=
3s
I
Droplets
Freezing

Cascade Freezing